

Myoelectric Control of a Soft Hand Exoskeleton Using Kinematic Synergies

Martin K. Burns ^{ID}, *Graduate Student Member, IEEE*, Dingyi Pei ^{ID}, *Student Member, IEEE*,
and Ramana Vinjamuri ^{ID}, *Senior Member, IEEE*

Abstract—Soft hand exoskeletons offer a lightweight, low-profile alternative to rigid rehabilitative robotic systems, enabling their use to restore activities of daily living (ADL) in those with hand paresis due to stroke or other conditions. The hand exoskeleton with embedded synergies (HEXOES) is a soft cable-driven hand exoskeleton capable of independently actuating and sensing 10 degrees of freedom (DoF) of the hand. Control of the 10 DoF exoskeleton is dimensionally reduced using three manually defined synergies in software corresponding to thumb, index, and 3-finger flexion and extension. In this paper, five healthy subjects control HEXOES using a neural network which decodes synergy weights from contralateral electromyography (EMG) activity. The three synergies are manipulated in real time to grasp and lift 15 ADL objects of various sizes and weights. The neural network's training and validation mean squared error, object grasp time, and grasp success rate were measured for five healthy subjects. The final training error of the neural network was $4.8 \pm 1.8\%$ averaged across subjects and tasks, with $8.3 \pm 3.4\%$ validation error. The time to reach, grasp, and lift an object was 11.15 ± 4.35 s on average, with an average success rate of 66.7% across all objects. The complete system demonstrates real time use of biosignals and machine learning to allow subjects to operate kinematic synergies to grasp objects using a wearable hand exoskeleton. Future work and applications are further discussed, including possible design improvements and enrollment of individuals with stroke.

Index Terms—Hand exoskeleton, kinematic synergies, neural networks, object grasping, soft robotics, wearable robotics.

I. INTRODUCTION

STROKE, spinal cord injury, and other conditions can lead to functional impairment of the hand in an exceptionally large number of individuals in the US and worldwide [1]–[3]. The loss of motor function severely impairs a person's ability to independently perform activities of daily living (ADL), leading to financial, mental, emotional, and social hardships for themselves and their loved ones [4].

Manuscript received June 26, 2019; revised September 6, 2019; accepted October 5, 2019. Date of publication October 28, 2019; date of current version December 31, 2019. This work was supported in part by the New Jersey Health Foundation (NJHF) under Grant PC 76-16, in part by the National Science Foundation (NSF) under Grant CHS-1845197, and in part by the Stevens Office of Innovation and Entrepreneurship Doctoral Fellowship. This paper was recommended by Associate Editor B. P. L. Lo. (*Corresponding author: Ramana Vinjamuri*.)

The authors are with the Sensorimotor Control Laboratory, Department of Biomedical Engineering, Stevens Institute of Technology, Hoboken, NJ 07030, USA (e-mail: mburns@stevens.edu; dpei@stevens.edu; ramana.vinjamuri@stevens.edu).

Color versions of one or more of the figures in this article are available online at <http://ieeexplore.ieee.org>.

Digital Object Identifier 10.1109/TBCAS.2019.2950145

Wearable robots capable of actuating an impaired hand offer to help these individuals in rehabilitative and assistive capacities. Numerous groups worldwide have produced hand exoskeletons using rigid constructions and linkages. The HANDEXOS/HX systems [5]–[7] are remote-actuated assistive devices which utilize compact pulley systems and self-aligning rotation axes using redundant joints. The Hand of Hope system [8], [9] uses linear actuators mounted on the back of the hand to independently actuate each finger for rehabilitation exercises. The ExoK'ab uses DC motors mounted on the fingers to drive 10 active degrees of freedom (DoF) in flexion and extension for rehabilitation [10]. The UT hand exoskeleton is a low-weight index/thumb rehabilitation device which uses remote DC actuators and a 3D printed parallel mechanism to actuate the hand [11], [12].

Rigid hand exoskeletons are readily modeled and controlled; however, they compromise hand component mass and size. This may be acceptable in the rehabilitation context, where such systems are mechanically supported and/or immobile. However, form factor and weight of the hand component are significant decision drivers for assistive devices with individuals with hand paresis [13], [14]. In response, many recent assistive hand exoskeletons are soft, lightweight systems [15], [16]. The ExoGlove Poly is a remote-actuated cable driven thumb/index/middle exoskeleton fabricated from silicone which is capable of two independently actuated DoF [17]. The Bioservo CarbonHand is a commercially available cable driven fabric exoskeleton which provides grasp assist for users with residual hand function [18]. Some designs use soft hydraulic or pneumatic actuators instead of motors and cables, such as the Wyss Soft Robotic Glove [19] and the ExoGlove [20]. The construction of soft exoskeletons relies on the user's bone structure to supply the rigidity and joint centers of rotation for effective motion. This causes the device dynamics to be heavily dependent on the user, leading to high model uncertainty and difficulty in accomplishing accurate control. For this reason, soft exoskeletons tend to be open-loop systems which don't incorporate sensor feedback from the finger joints. These wearable devices, as well as current prosthetics, can be controlled in many different ways, with promising progress using electromyography (EMG) [21]–[23].

The tradeoff between controllability and portability has major implications for dexterous control. For a device to adequately reproduce natural hand function it must have a high number of DoFs and have a controller which can coordinate those DoFs biomimetically, with minimal effort from the user. This equates



Fig. 1. HEXOES hand component, showing the dorsal spring-extension system and the flex sensor wiring.

to dimensionally reducing the controls problem: imposing a lower-dimensional control method onto the high-DoF system with minimal tradeoff in dexterity. In hand grasping research, this comes in the form of kinematic synergies, or “a collection of relatively independent degrees of freedom that behave as a single functional unit” [24]. Synergies derived from biomechanical hand grasping studies represent whole-hand movement patterns that best account for variance in grasping data, and so are hypothesized to act as building blocks of motion. Human hand grasping can be reproduced to an arbitrary accuracy by selecting fewer synergies than the number of DoFs of the controlled system [25]. This has been demonstrated in grasping [26]–[28], biometrics [29], and bilateral reaching [30].

Prior work on synergy-based brain machine interfaces (BMIs) has demonstrated that relatively few motion patterns can be used to control high DoF systems [26], even to replicate tasks of ADL [30]. Several groups have designed prosthetics and exoskeletons which mechanically implement synergies to control high-DoF hands with only one or two actuators [31]–[33]. These devices significantly simplify the control complexity of prosthetics, however the synergies they actuate cannot readily be modified. In this study we experimentally demonstrate the hand exoskeleton with embedded synergies (HEXOES), shown in Fig. 1, which is an iteration on the previous HEXOES model [34]. This 10-DoF soft whole-hand remote cable-driven exoskeleton uses software-defined kinematic synergies to dimensionally reduce the required control inputs. The high-DoF actuation allows us to easily change synergies or control methods, making this system novel and ideal for testing synergy-based controls. EMG signals from the contralateral arm control 3 pre-defined synergy profiles in real time using a trained neural network. Five healthy individuals are recruited to train the neural network and conduct an object grasping study using fifteen objects representative of ADL.

II. METHODS

In this experiment, healthy subjects were recruited to control HEXOES, worn on their right hand, using EMG signals from their left arm. Flexion/extension of the wrist and elbow and abduction/adduction of the shoulder of the left arm are

coordinated by the user and measured using the EMG sensors. A neural network was first trained to recognize the individual arm motions and their combinations, which were then used to control three manually defined kinematic synergies of the exoskeleton hand. Once the system was trained, subjects used the real-time open loop system to complete an object grasping study. All real-time algorithms, neural network training, and hardware communications were implemented in LabVIEW and MATLAB, with MATLAB used for offline analysis. The individual components of the system will be discussed in detail, followed by the experiment protocol.

A. Exoskeleton Design

HEXOES is composed of a lightweight hand assembly and a remote actuator assembly connected by a flexor bundle (Fig. 2). The actuator assembly contains ten L16 linear actuators (Actuonix, British Columbia, Canada) with a 20 mm/s no-load speed and 100N maximum linear force. Each actuator has a built-in potentiometer which measures linear position, ranging from 0.5 V to 4.5 V. Two Arduino Mega 2560 boards are used for analog data acquisition and PWM control of the motors. The total mass of the actuator assembly is 2.2 kg.

The glove-based soft hand (Fig. 3) provides active flexion and passive extension of the metacarpophalangeal (MCP) and proximal interphalangeal (PIP) joints of each finger and thumb of the right hand, totaling 10 independently actuated DoF. 3D printed compliant finger components fabricated from thermoplastic polyurethane (TPU) provide anchor points for the flexion and extension cables while allowing the exoskeleton’s fingers to stretch to fit different hand sizes. These soft deformable components allow a comfortable yet snug fit, increasing device usability. Flexion is actuated by ten nylon braided filament cables which run along the palm support of the hand and out through the flexor bundle, which contains ten polytetrafluoroethylene (PTFE) Bowden tubes. The palm support can be detached from the rest of the glove using a tongue-and-groove clasp locked with a cotter pin, and zippers along the sides of the palm allow the exoskeleton to be opened for donning and doffing. Passive extension of each joint is provided by adjustable springs on the dorsal side of the hand. The angle of each MCP and PIP [Fig. 3(c)] joint is measured using 2" and 1" Tactilus flex sensors (Sensor Products, New Jersey, USA) stitched into pockets on the back of the glove. The glove assembly weighs a total of 258 g.

B. Data Capture

1) *Kinematic Data:* Joint angles are recorded over time using two sets of data streams. The MCP and PIP flex sensors are measured using $33\text{ k}\Omega$ voltage dividers with a 4.5 V excitation voltage and digitized using an Arduino Mega. The actuator potentiometers are also recorded over time, allowing redundant joint angle measurement. For this work, the distal interphalangeal (DIP) joint is not independently measured as it is standard to approximate its motion as directly proportional to the PIP joint. A 60 Hz notch filter and 10-point moving average filter eliminate sensor noise.

2) *Electromyography:* EMG signals were measured at 2 kHz using a 16-channel Trigno wireless EMG system (Delsys, MA

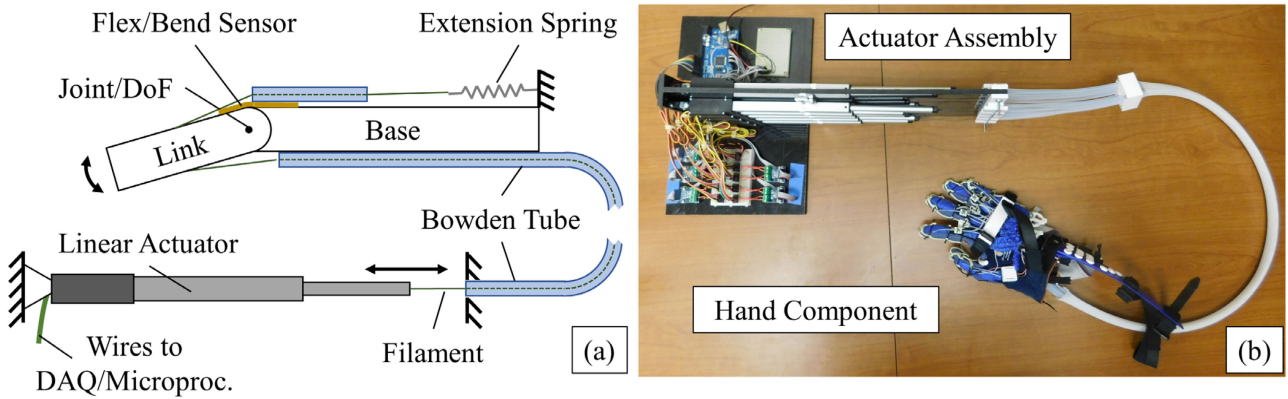


Fig. 2. (a) Actuation diagram of 1 DoF of HEXOES. A linear actuator pulls nylon filament through a Bowden tube which terminates on the palmar side of a joint. An extension filament attaches to a spring on the dorsal side of the joint which is fixed to the structure of the exoskeleton. (b) The HEXOES system with the hand component and remote actuator assembly visible.

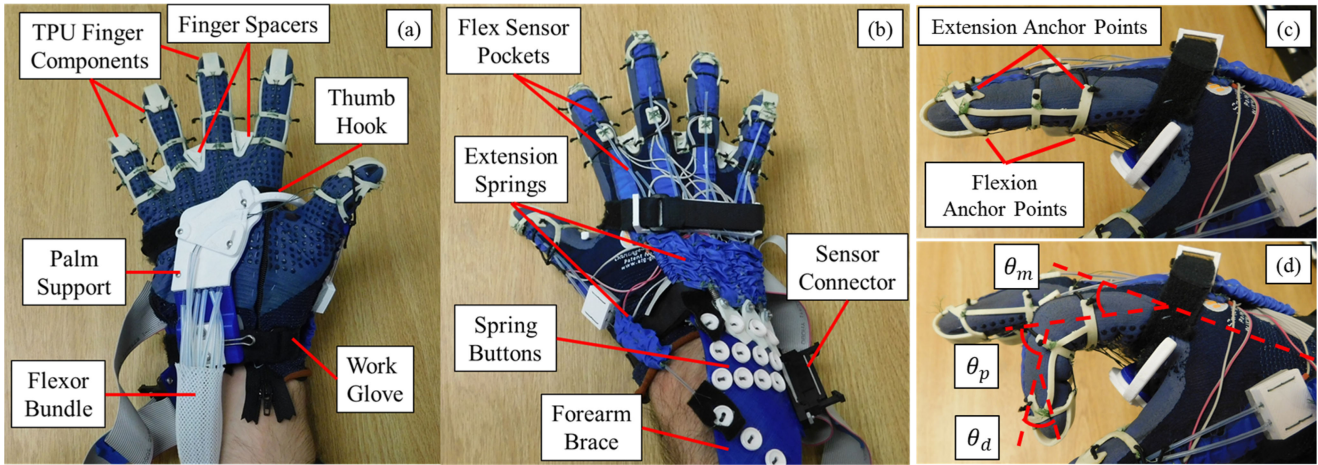


Fig. 3. Labeled components of HEXOES hand component. (a) Palmar side, with key features of the palm support and finger components labeled. (b) Dorsal side, with sensors and spring-retraction system labeled. (c) Lateral view of index finger with filament anchor points labeled. (d) Index finger flexed with θ_m , θ_p , and θ_d labeled for the MCP, PIP, and DIP joint angles respectively.

United States). Sensors were placed on six locations on the left arm according to Table I after light abrasion and cleaning of the site. Data was processed in real time by forming a 300-sample moving window (Fig. 4). This window was processed using a 20–500 Hz bandpass filter to remove movement artefacts, higher-frequency noise, and heartbeat, and a 60 Hz notch filter with a 0.5 Hz bandwidth for line interference, and a 200-sample moving average rectified value filter to stabilize the signal. An average of the window is computed every 150 samples to yield an input set for the neural network at a sample rate of 13.33 Hz. This sample rate was chosen to be rapid enough to be imperceptible to the user [35] while reducing noise in the measured signal.

C. Neural Network

The aim of this study was to use EMG signals from wrist, elbow, and shoulder flexion to control three synergies in an exoskeleton hand. Using these joint-level motions would be

mentally easier for the subject to coordinate than the equivalent individual muscle activations, an issue that is especially present in the affected population. However, these joint-level motions can result in unintended co-contractions of the muscles being instrumented, and these co-contractions can vary from subject to subject. This precludes the use of simple thresholds on muscle activity in favor of an algorithm that can learn these activation patterns. For this, a neural network is used. The neural network consists of a 6-element input layer, a hidden layer, and a 3-element output layer. The hidden layer consists of 8 elements with a sigmoid transfer function, and was designed prior to the experiment. The structure of the network was fixed for consistency during this experiment. The outputs of the neural network are continuous from -1 to $+1$, so a threshold of ± 0.5 is applied to each output element to produce either -1 , 0 , or $+1$. The thresholded outputs are used as a three-element synergy recruitment weight column vector, \bar{w} , to produce the 10-element motor power command vector, \bar{p} , ranging from -1 (extend) to $+1$ (flex) using a 3×10 synergy

TABLE I
EMG SENSOR POSITIONS

Motion	Sensor Number	Muscle
Wrist F/E	1	Flexor Carpi Radialis
	2	Extensor Carpi Ulnaris
Elbow F/E	3	Biceps Brachii
	4	Triceps Brachii Lateral Head
Shoulder Abd/Add	5	Pectoralis Major (Clavicular Region)
	6	Medial Deltoid

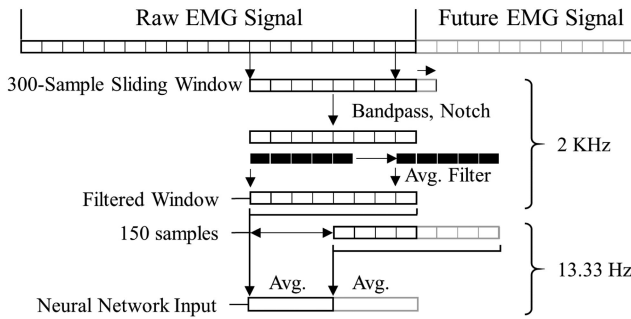


Fig. 4. EMG processing scheme from raw data to neural network inputs. A 300 sample sliding window is filtered using a bandpass, notch, and 200-sample moving average filter. The average of the filtered 300-sample window is computed every 150 samples, yielding the neural network inputs at a final sample rate of 13.33 Hz. This was performed for each EMG channel.

matrix S :

$$\bar{p} = S\bar{w} \quad (1)$$

In this scheme, the first element of \bar{w} controls thumb flexion and extension, the second element controls index flexion and extension, and the third element controls flexion and extension of the remaining three fingers. The S matrix is manually set to generate these motions when the corresponding weight is activated.

D. Neural Network Training

The neural network is trained such that the thumb is controlled by the shoulder, the index finger is controlled by the elbow, and the remaining fingers are controlled by the wrist. Training tasks were accumulated for the neural network in alternating rest/task pairs, an example of which is shown in Fig. 5. Three random rest samples (red dots) are selected from the interval before the task prompt is given, shown as the blue dotted line. An automated prompt tells the subject to flex their wrist, resulting in the processed wrist flexor EMG activity shown in black as the first neural network input. A K-means clustering algorithm is applied to all channels of the data during this task, which separates the recorded data into three clusters. K-means allows automatic data separation which adapts to different activation amplitudes without the need to manually tune an activation threshold. C-1 identifies transient activation spikes in the data, C-2 identifies the sustained task activation, and C-3 identifies the signal's resting state. Three task samples are isolated from C-1 and C-2 at random with a spacing buffer as the task samples. The resting and task samples are paired with the corresponding

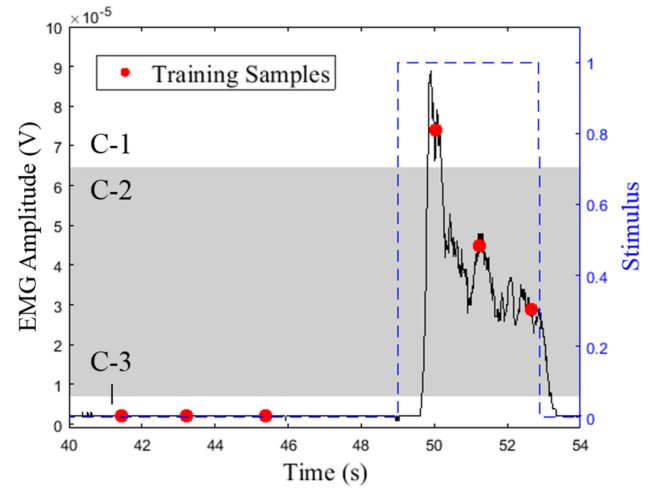


Fig. 5. Isolation of EMG training samples using K-means clustering. The stimulus given to the subject (blue) elicits the processed EMG response (black). Three clusters are identified corresponding to the transient activation spike (C-1), the sustained activation (C-2), and the resting signal (C-3) shown as alternating white/gray regions. Three random samples shown in red circles are isolated from each rest period and each activation.

neural network output targets for training, and the process is repeated for every training task in the experiment. The neural network is trained using a Bayesian regularization algorithm, which minimizes the network's internal parameters and model error to avoid overfitting.

E. Subjects

Subjects were recruited under an approved protocol overseen by the Stevens Institute of Technology IRB, in accordance with the Helsinki Declaration. Five healthy subjects age 24.8 ± 2.8 years, 4 male and 1 female, were recruited for this experiment after giving their informed consent. Three subjects were self-reported right-handed. Subjects were all naïve to EMG-based myoelectric interfaces and had no prior injuries that affect hand or arm function.

F. Experiment Protocol

Upon arrival, subjects signed the necessary consent documents and were fitted with the EMG sensors described above. Sensor locations on each muscle were manually probed until a visually discernable signal was measured during isometric contraction. The subject then donned the exoskeleton, and the experimenter-controlled calibration process was executed. The experiment consists of three phases conducted in one session. Phases one and two collect training data for the neural network, while phase three consists of object grasping using the EMG-driven exoskeleton without assistance or guidance.

Each of the first two phases consist of two sets of six arm contraction tasks. The first set of tasks are performed for four repetitions and are used to accumulate training data for the neural network. The second set of tasks are performed for three repetitions and are used as a validation dataset for the final model. Each repetition of each task consists of approximately 3

seconds of rest, followed by approximately three seconds of arm contraction. Successful rest and contraction tasks are manually marked by button press by the experimenter. The exoskeleton actuates according to the synergy corresponding to that task when the experimenter cues a successful arm contraction. In phase one, the six contraction tasks are shoulder adduction, shoulder abduction, elbow flexion, elbow extension, wrist flexion, and wrist extension. In phase two, the six contraction tasks are simultaneous contractions of multiple joints, chosen based on their corresponding grasping scheme. Simultaneous shoulder and elbow flexion and extension is trained for an index/thumb precision grasp, shoulder and wrist flexion and extension are trained for a thumb and three-finger grasp, and shoulder, elbow, and wrist flexion and extension are trained for a whole-hand grasp. In total, the training set consists of 144 rest samples, 72 single-contraction samples (12 for each of six possible motions), and 72 simultaneous contractions (12 for each of six included motions). At the end of phase two, the neural network is fully trained and an independent validation dataset has been accumulated for single and simultaneous contractions.

Phase three of the study is the object grasping phase. The subject sits at a table with the exoskeleton hand resting palm-down in a 25 cm × 15 cm rest area, aligned with the subject-side edge of the table. The object is placed 35 cm away from the edge of the table centered on the subject. The subject is given a verbal start cue, at which point they reach for the object and begin using their contralateral arm to operate their hand. Subjects pick up the object to signify a successful grasp, place it back on the table, use their contralateral arm to release the object, and return to the resting position. The experimenter uses a keyboard input to mark the time from a successful object lift to the subject returning their hand to the rest area. Subjects are instructed to maintain light finger extension in their right hand during object grasping. This serves as a simple cue for the subject that ensures there is no subconscious grasp assistance to the exoskeleton. In the event of an unsuccessful grasp, subjects are instructed to continue with the release and return phase as if the grasp was a success. Fifteen objects are grasped: A large handle, a pencil eraser, a dry erase marker laid flat on the table, a baseball, a dish sponge, a wooden spoon, a 2" × 2.5" × 2" foam block, a roll of painter's tape, a 1" triangle of foam, a coffee mug handle, a wooden nut and bolt, a full water bottle (492 g mass), a full spray bottle (920 g mass), an empty soda can, and a screw driver. Each object is grasped in this order, and the sequence is repeated for three repetitions.

G. Experiment Metrics

Kinematic data and EMG signals are recorded during all phases of the experiment. The neural network is trained after the first set in phases one and two. The network's training performance, measured as training mean-squared error (MSE_T) as generated by the Bayesian regularization algorithm, is recorded for the single contraction training (phase one) and the combined single/simultaneous contraction training (phase two). The neural network's performance is computed as the mean squared error (MSE_V) between the task stimulus, $\bar{s}(t)$, and the neural

TABLE II
OBJECT GRASP CATEGORIES

Precision	Cylinder	Whole-hand/spherical
Pencil eraser	Handle	Ball
Dry-erase marker	Spoon	Foam (large)
Tape roll	Mug	Nut & bolt
Foam (small)	Water bottle	Screwdriver
	Spray bottle	Sponge
	Soda can	

network's output, $\bar{w}(t)$, of a given validation task

$$MSE_V = \frac{1}{T} \sum_{t=1}^T (\bar{s}(t) - \bar{w}(t))^2 \quad (2)$$

and is computed for each output and individual validation task of phase one and two. Grasp success, measured as ability to lift the object off the table without dropping it, time to pick up object, and task completion time are also measured for each repetition of each object as high-level task metrics. We also compute the fraction of synergy recruitments used during each object grasp, f_i :

$$f_i = \frac{\sum_{t=0}^T |w_i(t)|}{\sum_{i=1}^3 \sum_{t=0}^T |w_i(t)|} \quad (3)$$

where $w_i(t)$ is the i^{th} recruitment weight at time t . This method ignores the resting or no-recruitment samples and so focuses on the absolute relative recruitment of each synergy. We group the objects into three broad categories based on the three types of grasps expected: precision grasps, cylinder grasps, and whole-hand/spherical grasps (Table II). This is done in accordance with accepted grasp taxonomies [36], [37]. The synergy recruitment fractions are compared between grasp types.

III. RESULTS

A. Neural Network Training

MSE_T is reported as the mean-squared error between the trained neural network output for the training dataset and its expected output. For single-contraction training, the neural network yielded an MSE_T of 0.048 ± 0.018 across subjects while the final network trained on single and combined contractions had an MSE_T of 0.048 ± 0.013 .

After training, the neural network was evaluated with separate real-time validation tasks for both single and combined contractions. Fig. 6 shows one set of validation tasks for subject 1. In this task, the subject performed shoulder abduction and wrist extension, corresponding to values of -1 in the blue plot. Activation of the lateral deltoid (Syn. 1 EMG) and wrist extensor bundle (Syn. 3 EMG) are visible, with coactivation of the biceps brachii in the elbow (Syn. 2 EMG). The neural network output, shown as gray circles, is overlaid on the expected output in blue. Except for three samples the neural network was able to correctly classify Syn. 2 as inactive. The MSE_V for this task averaged across outputs is 0.0394. The mean MSE_V across subjects, outputs, and tasks is 0.066 ± 0.045 for single-contraction validation and 0.083 ± 0.034 for combined contraction validation.

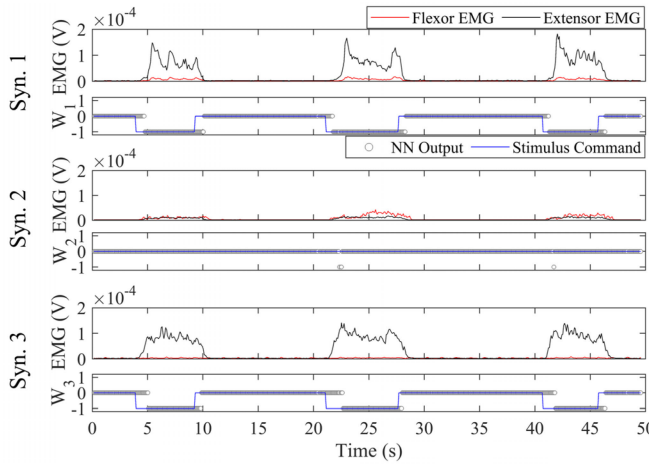


Fig. 6. Subject 1 phase two validation dataset for task 4. Shoulder abduction and wrist extension are performed for three rest-task repetitions. Filtered EMG signals from the flexor (red) and extensor (black) muscles are input into the neural network. The output (gray circles) are compared to the stimulus (blue) to compute MSE_V . Co-contraction of the elbow muscles (Syn. 2) are visible in the data, however the model can still correctly classify the output.

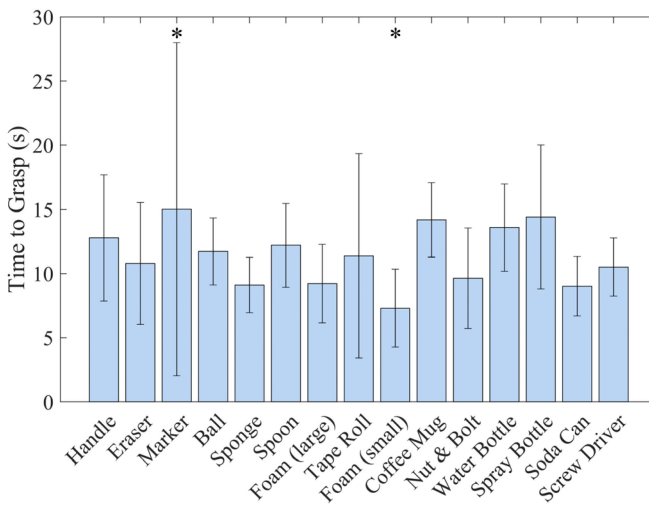


Fig. 7. Object grasping time averaged across subjects and repetitions. The object numbers correspond to the object order listen in the experiment protocol section.

B. Object Grasping

Object grasping time, defined as the time between movement onset and object pickup, was averaged across subjects and repetitions. These results are shown in Fig. 7. The fastest object grasps were object 9, the small foam triangle (7.31 ± 3.04 s), and object 14, the empty soda can (9.02 ± 2.31 s). Object 3, the dry erase marker, has a large standard deviation and inflated mean due to an extreme outlier of 54.47 s. With this outlier removed, the grasp time for object 3 changes from 15.02 ± 12.97 s to 11.43 ± 3.9 s. The object with the longest mean grasp time (outlier removed) was object 13, the 920 g spray bottle at 14.4 ± 5.61 s. The global mean object grasping time across objects, repetitions, and subjects is 11.15 ± 4.35 s excluding the outlier. An

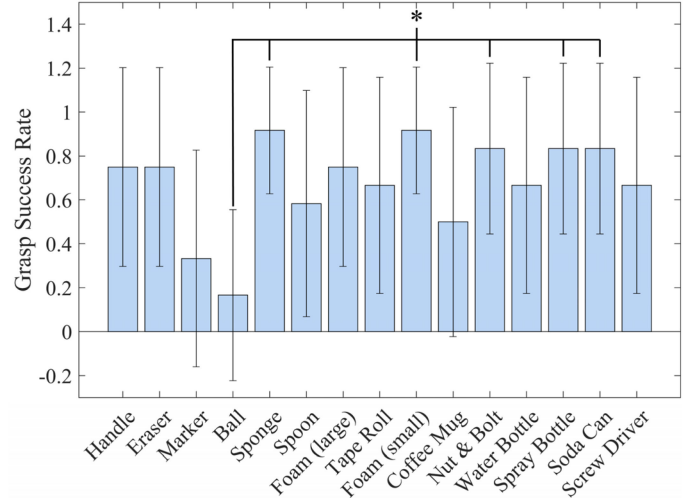


Fig. 8. Object grasp success rate across subjects and repetitions. A statistically significant difference was found between the ball and the sponge, small foam triangle, nut & bolt, spray bottle, and soda can ($p = 0.001$).

ANOVA comparison between objects with $\alpha = 0.05$ revealed significant differences in object grasp times ($p = 0.004$), with outliers removed. A tukey-kramer post-hoc analysis showed a significant difference between the grasp times of the marker and the small foam triangle, with all other grasp times being statistically similar. The mean task completion time is 21.92 ± 7.16 s.

The grasp success rate (Fig. 8) is an interesting metric for determining candidate objects for grasp studies with individuals with stroke. Successful repetitions for all subjects are pooled to get an overall success rate for each object. The most successfully grasped objects are objects 5 and 9 which are the dish sponge and small foam triangle, respectively. Each of these objects had a 91.7% success rate with only one missed repetition across subjects. The worst-performing object was the baseball, with only two successful grasps across all subjects, or a 16.7% success rate. The mean and mode of the grasp success rate was 67.8% and 66.7%, respectively. An ANOVA analysis with tukey-kramer post-hoc reveals a significant difference between the lowest success rate (ball grasp) and the highest success rates (sponge, small foam triangle, nut & bolt, spray bottle, and soda can) with $\alpha = 0.05$.

The synergy recruitment fractions were computed for each repetition, task, and subject and were pooled into the three grasp categories in Table II. The results are shown in Fig. 9, with each group of bars representing each grasp type and each sub-bar representing synergy recruitment. Two-way unbalanced ANOVA with grasp type and synergy number as groups revealed no statistical difference across grasp types ($p \gg 0.05$), meaning there was a roughly equal recruitment averaged across synergies within each grasp type. A significant difference was found across synergies ($p \ll 0.05$), with post-hoc analysis showing all three synergies had significantly different levels. Synergy 1, controlling the thumb, was recruited the most followed by synergy 2 with the index finger and synergy 3 with fingers 2–4. A significant interaction was also found between grasps and synergies

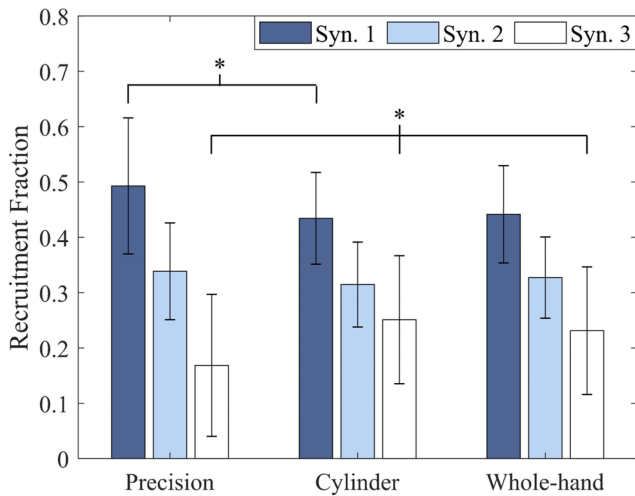


Fig. 9. Recruitment fraction, f_i , for the i th synergy compared across grasp type. No significant difference was found across grasp type ($p \gg 0.05$). Significant differences were found across synergies ($p \ll 0.05$). Significant interactions between grasps and synergies resulted in significant differences between synergy 1 recruitment in precision grasps and in cylinder grasps. Synergy 3 was recruited significantly less in precision grasps than in whole-hand/spherical and cylinder grasps.

($p \ll 0.05$), meaning that the synergy recruitment fraction was affected by grasp type. Post-hoc analysis of the interaction reveals several trends. Synergy 2 was statistically equivalent across all grasp types, meaning the index finger was recruited equally across precision, cylinder, and whole-hand grasps. Synergy 1 was recruited significantly higher in precision grasp than in cylinder grasps but was similar to whole-hand/spherical grasps. Synergy 3 was significantly lower in the precision grasp than in both the cylinder and whole-hand/spherical grasps, which is an expected result. There was no difference found between cylinder and whole-hand/spherical grasps within synergies.

C. Exoskeleton Kinematics

A sample of the kinematics, EMG signals, and synergy recruitment is shown in Fig. 10. The different motion phases (resting, grasping, object pickup, releasing, and return) are visible in the kinematic data, however sensor placement issues cause some sensors to not detect motion. Four such sensors are visible in this sample data, with other subjects missing two active sensors, which tend to be the pinky sensors.

IV. DISCUSSION

This paper presents a soft cable actuated 10-DoF whole-hand exoskeleton meant to be an assistive device for individuals with stroke. We demonstrate an open-loop control system where a neural network interprets EMG signals in the contralateral arm to actuate three synergy motions of the hand. The synergies correspond to independent flexion and extension of the thumb, index, and remaining three fingers. Subjects can operate this system to grasp objects ranging from a pencil eraser to a full spray bottle weighing approximately 1kg without assisting the glove.

As a usability study, this work verifies that the HEXOES device is a functional object grasp system that meets requirements for safety, device mass, and donning/doffing, while offering high-DoF actuation and sensor feedback. The use of kinematic synergies enables complex high-DoF biomimetic movement patterns operated through the low-DoF synergy recruitment domain. Adaptive algorithms, such as the neural network shown here, are used to map biosignals, such as EMG, to the synergy recruitment domain. The next steps in the development of HEXOES will be to extend subject recruitment to include individuals with stroke with minimal residual hand function. We will also experiment with postural and spatiotemporal synergies to evaluate their use as assistive grasping controls. Finally, we will implement a model-driven closed-loop control system, however this will require several advances to first occur.

The synergy control method shown here uses EMG signals of the unaffected arm to drive hand motion of the affected arm. We use an automated training system to learn the muscle activation patterns corresponding to three bidirectional control commands without the need for manual tuning or adjusting thresholds. The motions of the contralateral arm were chosen as distinct motions that use the unaffected motor pathway for the upper limb. This approach is supported by prior findings where the brain manages to learn interlimb motor mappings, especially in the presence of proprioceptive feedback [38]. These motions serve the purpose of a lab-controlled grasping study, however in real applications this approach could impair the use of a patient's unaffected arm, or lead to false control signals being sent to the exoskeleton. Future work on the assistive system will explore optimal EMG sensor placement and leverage control movements that are intuitive for individuals with Stroke. Such a system can use the same machine learning system as shown here to derive synergy commands. Once determined, subjects could practice driving the system with either the exoskeleton or with virtual reality environments.

The primary design requirements for assistive hand exoskeletons concern wearability and ease of use. The mass of the hand component must be light enough that an individual with hand impairment can lift, move, and position themselves for object grasping. This mass was suggested to be 0.5 kg [35], which is roughly equivalent to the mass of the average adult male hand [39]. Any external hardware such as a remote actuation unit must also weigh less than 3 kg [35]. In addition, the assistive system should be controllable through biosignals or kinematics, must supply adequate force to perform ADL, must be minimally complex, comfortable to wear, easy to don/doff, provide close to a healthy range of motion, produce smooth responses to control inputs, be safe to use, and be low enough in cost to be available to the population [40], [41]. Rigid systems such as the Hand of Hope [8], [9] meet many of these design criteria, particularly for controllability, range of motion, and force to execute ADL, however the rigid mechanisms tend to make the devices too heavy to be worn as an assistive system. Soft exoskeletons such as the Wyss Soft Robotic Glove [19] and the ExoGlove Poly [17] use an alternative approach, adapting intrinsically soft design and low-DoF control to achieve functional grasping systems with minimal worn weight. With this approach, these low-DoF

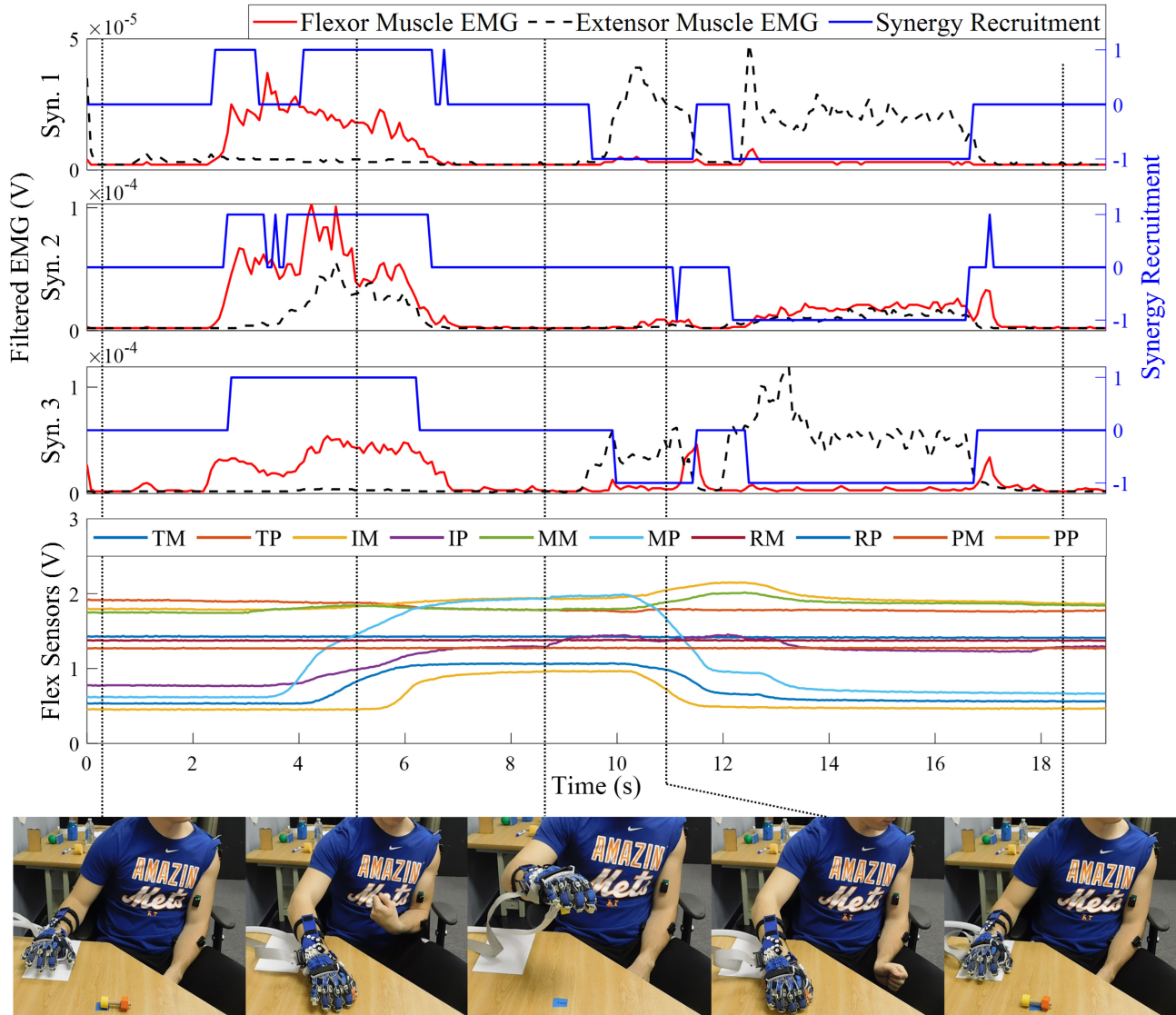


Fig. 10. Subject 3 performing a reach and grasp task for object 11, the nut and bolt. The filtered EMG signal, in Volts, for the flexor (solid red) and extensor (black dotted) muscles are shown for each synergy (Syn. 1–Syn. 3) along with the resulting synergy recruitment, in blue. Exoskeleton sensor measurements in Volts are shown below, showing a clear grasp, hold, and release period. Joints are labeled in the exoskeleton sensor plot in finger-joint pairs, e.g., TM stands for thumb MCP and RP stands for ring PIP. Grasp events are shown along the bottom, with the corresponding time in the data.

systems meet the design criteria but may sacrifice their dexterity, placing a limit on the performance they can achieve for object grasping and manipulation.

HEXOES aims to match the dexterity of the hand as closely as possible while meeting the design criteria that outline a practical assistive device. The system is easy to don and doff, with a zipper and clasp system which allows the palmar side of the hand component to open. This makes the glove-based design easy to wear on a paralyzed hand. We incorporate 10 independently actuated DoF, more than other devices in the literature, to finely control hand postures and motion. The increased DoF lead to higher device complexity in both mechanical design and user control, however we address this tradeoff in several ways. Mechanically, we sought a simple design for a single DoF, which minimizes the parts and mechanisms needed to actuate the hand. The reduced part count leads to fewer points of failure, as well as

a significantly reduced total mass. The 10 DoF hand component and actuator assembly of HEXOES weighs 258 g and 2.2 kg respectively, coming in significantly lower than the 0.5 g and 3 kg criteria. The increased DoF would lead to a higher control burden on the user, however by employing a synergy-based control method we can minimize the effort needed to operate a dexterous system while maintaining the system's dexterity.

This paper proposes a control scheme based on spatial or postural kinematic synergies. The three actuated synergy profiles were manually defined as orthogonal motion of the thumb, index, and remaining three fingers. These were chosen as easily coordinated motions while still allowing formation of pinch, key, handle, and whole-hand grasps. Biomechanically derived spatial synergies, such as those extracted from grasp data [28], [42], [43], can easily be integrated by modifying S . Spatial synergies are concise, represent hand postures well, and are

easy to integrate into traditional control methods. Numerous other groups have demonstrated similar controllers based on postural synergies for autonomous object grasping [44]–[46] as well as prosthetics/robotic control [47]–[51]. These range from open-loop systems using positional control at the joint level to impedance controllers which operate in the synergy recruitment domain. Whereas spatial synergies encode relative joint movements that are fixed in time and are derived from end-postures of object grasps, spatiotemporal synergies allow these relative motions to vary across the duration of the synergy. This allows them to capture the dynamic trajectory the hand follows during reaching and grasping, and so may capture more information on hand motion. Spatiotemporal synergies have been used to computationally reconstruct hand grasps [52], [53] and bilateral reaching and manipulations [30] to a high accuracy, and have also been mechanically implemented into a two-synergy anthropomorphic prosthetic hand [31]. The next steps in this project will be to develop a control system that operates using spatiotemporal synergies, which would be one of the first made. This should enable greater dexterity and object manipulation while still using as few as one or two control inputs.

Soft robotic hand exoskeletons rely on the user's anatomy to provide the structure for proper function, and so their dynamics are heavily influenced by the user's hand. The compliant nature of the system leads to high uncertainty in geometric parameters (filament anchor points, sensor locations, etc.) which will change over time with component deformation. This would include both short-term changes over individual flexion/extension motions and long-term changes over the course of a session or over the span of hours. There are many unknown variables that must be determined to get a full controllable system, so identifying an adequate model of the exoskeleton and hand system is essential work that will be pursued as next steps. This includes not only geometric parameters but dynamic effects from line friction, extension forces, and the effect of contact forces between the tendon lines and grasped objects. It is also possible that the grasp times and success rates measured here are sensitive to hand size. The early results shown here appear to support this, however more subjects must be recruited to achieve a statistical result. If found to be significant, then hand components designed for different hand sizes may be produced and used with the same actuator assembly.

Sensor accuracy is essential to create a controllable robotic system, yet there is no reliable method of sensing hand joint angles with soft systems. The actuation of soft systems results in bending or compliant deformation of the device members, as opposed to rotation of linkages in rigid mechanisms. This precludes the use of traditional angle sensors such as potentiometers or encoders without incorporating rigid hardware. Because of this, sensors that detect bending and deformation offer a logical solution to the sensor issue, especially considering the commercial availability of bendable flex sensors. Indeed, several commercial devices such as the CyberGlove (CyberGlove Systems LLC, San Jose, CA, USA), 5DT Glove (5DT Technologies, Pretoria, ZA), Data Glove (Performancemesh, UK), and the VMG 30 data glove (Virtual Realities LLC, League City, TX, USA) all operate using flex-sensing fiber optics or printed electronics. Sensor

gloves in research, such as those produced by [54]–[56], also use flex sensors. The major drawback to these sensors, which has been extensively noted in the cited literature, is that they are susceptible to several different kinds of variation which impedes their use in joint angle sensing. There is variability between sensors in the electrical resistances supplied, their sensing regions are susceptible to damage, affecting their performance, the wire connections tend to degrade from repeated bending, and they are prone to placement error on the glove. In this study we observe sensor placement issues on the exoskeleton, where the sensing region of some (fewer than 3) flex sensors are not located over the joint and so no change in signal is observed over the range of motion. Moving forward, we expect to incorporate the flex sensors and actuator potentiometer measurements into a model for the exoskeleton joint angles, however a full treatment of this approach will be examined in future work. Once a robust angle sensing system is in place, the exoskeleton can be operated by a full closed-loop control system.

Additional improvements to HEXOES can increase its usability. The object grasp results shown here reveal that some design changes can be made to allow easier object grasping. For instance, the palm support can be revised to interfere less with the hand's workspace, which would lead to improved grasps on the ball. Future design iterations can further reduce the mass and size of both the hand component and the actuator assembly. The actuator assembly can also be condensed into a backpack or hip bag or can be mounted on a platform such as a wheelchair or mobility scooter. The hand component is already light enough for those with residual arm function to use, however coupling the device with a wrist or forearm assist device could allow those with total paralysis to benefit from HEXOES. Since the hand component is predominantly 3D printed, we can investigate methods of personalized design and fabrication so that the system can be custom-fit to the user. We can also explore more durable materials, yielding a highly robust device aimed at dexterously assisting those with paralysis. Additionally, the data monitored by HEXOES could be used to evaluate hand function in those who suffer stroke, spinal cord injury, or traumatic brain injury. Joint range of motion, fluidity of movement, muscle fatigue, and measures of degree of assistance could all be tracked by clinicians.

V. CONCLUSION

This paper demonstrates HEXOES as an open-loop assistive robotic exoskeleton which uses biosignals to control hand synergies. Healthy individuals were recruited to control the system with their contralateral arm while maintaining a limp hand. Subjects were able to grasp and lift objects indicative of ADL. These objects ranged from small objects requiring precise coordination, and large heavy objects which needed a powerful grip force with the flexibility to conform to irregular shapes. Future directions are discussed including enrollment of individuals with stroke, extension to recruitment of spatiotemporal synergies, model development with closed-loop control, and refining sensor feedback for joint angle estimation.

REFERENCES

- [1] V. Y. Ma, L. Chan, and K. J. Carruthers, "The incidence, prevalence, costs and impact on disability of common conditions requiring rehabilitation in the US: Stroke, spinal cord injury, traumatic brain injury, multiple sclerosis, osteoarthritis, rheumatoid arthritis, limb loss, and back pain," *Arch. Phys. Med. Rehabil.*, vol. 95, no. 5, pp. 986–995, 2014.
- [2] P. A. Heidenreich *et al.*, "Forecasting the future of cardiovascular disease in the United States: A policy statement from the American Heart Association," *Circulation*, vol. 123, no. 8, pp. 933–944, 2011.
- [3] V. L. Feigin *et al.*, "Global and regional burden of stroke during 1990–2010: Findings from the global burden of disease study 2010," *Lancet*, vol. 383, no. 9913, pp. 245–255, 2014.
- [4] A.-C. Jonsson, I. Lindgren, B. Hallstrom, B. Norrving, and A. Lindgren, "Determinants of quality of life in stroke survivors and their informal caregivers," *Stroke*, vol. 36, no. 4, pp. 803–808, 2005.
- [5] A. Chiri *et al.*, "HANDEXOS: Towards an exoskeleton device for the rehabilitation of the hand," in *Proc. IEEE/RSJ Int. Conf. Intell. Robot. Syst.*, 2009, pp. 1106–1111.
- [6] A. Chiri, N. Vitiello, F. Giovacchini, S. Roccella, F. Vecchi, and M. C. Carrozza, "Mechatronic design and characterization of the index finger module of a hand exoskeleton for post-stroke rehabilitation," *IEEE/ASME Trans. Mechatronics*, vol. 17, no. 5, pp. 884–894, Oct. 2012.
- [7] S. R. Soekadar *et al.*, "Hybrid EEG/EOG-based brain/neural hand exoskeleton restores fully independent daily living activities after quadriplegia," *Sci. Robot.*, vol. 1, no. 1, p. eaag3296, 2016.
- [8] N. S. K. Ho *et al.*, "An EMG-driven exoskeleton hand robotic training device on chronic stroke subjects: Task training system for stroke rehabilitation," in *Proc. IEEE Int. Conf. Rehabil. Robot.*, 2011, pp. 1–5.
- [9] Z. Lu, R. K. Y. Tong, X. Zhang, S. Li, and P. Zhou, "Myoelectric pattern recognition for controlling a robotic hand: A feasibility study in stroke," *IEEE Trans. Biomed. Eng.*, vol. 66, no. 2, pp. 365–372, Feb. 2019.
- [10] O. Sandoval-Gonzalez *et al.*, "Design and development of a hand exoskeleton robot for active and passive rehabilitation," *Int. J. Adv. Robot. Syst.*, vol. 13, no. 2, pp. 1–12, 2016.
- [11] P. Agarwal, J. Fox, Y. Yun, M. K. O'Malley, and A. D. Deshpande, "An index finger exoskeleton with series elastic actuation for rehabilitation: Design, control and performance characterization," *Int. J. Robot. Res.*, vol. 34, no. 14, pp. 1747–1772, 2015.
- [12] Y. Yun, P. Agarwal, J. Fox, K. E. Madden, and A. D. Deshpande, "Accurate torque control of finger joints with UT hand exoskeleton through Bowden cable SEA," in *Proc. IEEE/RSJ Int. Conf. Intell. Robots Syst.*, 2016, pp. 390–397.
- [13] S. Ates, C. J. W. Haarman, and A. H. A. Stienen, "SCRIPT passive orthosis: Design of interactive hand and wrist exoskeleton for rehabilitation at home after stroke," *Auton. Robots*, vol. 41, no. 3, pp. 711–723, 2017.
- [14] B. W. Gasser, D. A. Bennett, C. M. Durrough, and M. Goldfarb, "Design and preliminary assessment of Vanderbilt hand exoskeleton," in *Proc. IEEE Int. Conf. Rehabil. Robot.*, 2017, pp. 1537–1542.
- [15] C. Y. Chu and R. M. Patterson, "Soft robotic devices for hand rehabilitation and assistance: A narrative review," *J. Neuroeng. Rehabil.*, vol. 15, no. 1, pp. 1–14, 2018.
- [16] T. Shahid, D. Gouwanda, S. G. Nurzaman, and A. A. Gopalai, "Moving toward soft robotics: A decade review of the design of hand exoskeletons," *Biomimetics*, vol. 3, no. 3, p. 17, 2018.
- [17] B. B. Kang, H. Lee, H. In, U. Jeong, J. Chung, and K. J. Cho, "Development of a polymer-based tendon-driven wearable robotic hand," in *Proc. IEEE Int. Conf. Robot. Automat.*, Jun. 2016, pp. 3750–3755.
- [18] M. Nilsson, J. Ingvast, J. Wikander, and H. Von Holst, "The soft extra muscle system for improving the grasping capability in neurological rehabilitation," in *Proc. IEEE-EMBS Conf. Biomed. Eng. Sci.*, Dec. 2012, pp. 412–417.
- [19] L. Cappello *et al.*, "Assisting hand function after spinal cord injury with a fabric-based soft robotic glove," *J. Neuroeng. Rehabil.*, vol. 15, no. 1, pp. 1–10, 2018.
- [20] H. K. Yap, J. H. Lim, F. Nasrallah, J. C. H. Goh, and R. C. H. Yeow, "A soft exoskeleton for hand assistive and rehabilitation application using pneumatic actuators with variable stiffness," in *Proc. IEEE Int. Conf. Robot. Automat.*, Jun. 2015, pp. 4967–4972.
- [21] D. K. Kumar, B. Jelfs, X. Sui, and S. P. Arjunan, "Prosthetic hand control: A multidisciplinary review to identify strengths, shortcomings, and the future," *Biomed. Signal Process. Control*, vol. 53, 2019, Art. no. 101588.
- [22] M. Ergeneci, K. Gokcesu, E. Ertan, and P. Kosmas, "An embedded, eight channel, noise canceling, wireless, wearable sEMG data acquisition system," *IEEE Trans. Biomed. Circuits Syst.*, vol. 12, no. 1, pp. 68–79, Feb. 2018.
- [23] K. Gokcesu, M. Ergeneci, E. Ertan, and H. Gokcesu, "An adaptive algorithm for online interference cancellation in EMG sensors," *IEEE Sensors J.*, vol. 19, no. 1, pp. 214–223, Jan. 2019.
- [24] M. T. Turvey, "Action and perception at the level of synergies," *Human Movement Sci.*, vol. 26, no. 4, pp. 657–697, 2007.
- [25] M. Santello, G. Baud-Bovy, and H. Jörnstell, "Neural bases of hand synergies," *Frontiers Comput. Neurosci.*, vol. 7, pp. 1–15, Apr. 2013.
- [26] R. Vinjamuri *et al.*, "Toward synergy-based brain-machine interfaces," *IEEE Trans. Inf. Technol. Biomed.*, vol. 15, no. 5, pp. 726–736, Sep. 2011.
- [27] C. R. Mason, J. E. Gomez, and T. J. Ebner, "Hand synergies during reach-to-grasp," *J. Neurophysiol.*, vol. 86, no. 6, pp. 2896–2910, 2001.
- [28] M. Santello, M. Flanders, and J. F. Soechting, "Postural hand synergies for tool use," *J. Neurosci.*, vol. 18, no. 23, pp. 10105–10115, 1998.
- [29] V. Patel, M. Burns, R. Chandramouli, and R. Vinjamuri, "Biometrics based on hand synergies and their neural representations," *IEEE Access*, vol. 5, pp. 13422–13429, Jun. 2017.
- [30] M. K. Burns, V. Patel, I. Florescu, K. V. Pochiraju, and R. Vinjamuri, "Low-dimensional synergistic representation of bilateral reaching movements," *Frontiers Bioeng. Biotechnol.*, vol. 5, pp. 1–15, Feb. 2017.
- [31] W. Chen, C. Xiong, and S. Yue, "Mechanical implementation of kinematic synergy for continual grasping generation of anthropomorphic hand," *IEEE/ASME Trans. Mechatronics*, vol. 20, no. 3, pp. 1249–1263, Jun. 2015.
- [32] M. G. Catalano, G. Grioli, E. Farnioli, A. Serio, C. Piazza, and A. Bicchi, "Adaptive synergies for the design and control of the Pisa/IIT SoftHand," *Int. J. Robot. Res.*, vol. 33, no. 5, pp. 768–782, 2014.
- [33] K. Xu, Z. Liu, B. Zhao, H. Liu, and X. Zhu, "Composed continuum mechanism for compliant mechanical postural synergy: An anthropomorphic hand design example," *Mech. Mach. Theory*, vol. 132, pp. 108–122, 2019.
- [34] M. K. Burns, K. Van Orden, V. Patel, and R. Vinjamuri, "Towards a wearable hand exoskeleton with embedded synergies," in *Proc. Annu. Int. Conf. IEEE Eng. Med. Biol. Soc.*, 2017, pp. 213–216.
- [35] P. Polygerinos, Z. Wang, K. C. Galloway, R. J. Wood, and C. J. Walsh, "Soft robotic glove for combined assistance and at-home rehabilitation," *Robot. Auton. Syst.*, vol. 73, pp. 135–143, 2015.
- [36] T. Feix, J. Romero, H. B. Schmidmayer, A. M. Dollar, and D. Kragic, "The GRASP taxonomy of human grasp types," *IEEE Trans. Human-Mach. Syst.*, vol. 46, no. 1, pp. 66–77, Feb. 2016.
- [37] F. Stival, S. Michieletto, M. Cognolato, E. Pagello, H. Müller, and M. Atzori, "A quantitative taxonomy of human hand grasps," *J. Neuroeng. Rehabil.*, vol. 16, no. 1, pp. 1–17, 2019.
- [38] T. Pistohl, D. Joshi, G. Ganesh, A. Jackson, K. Nazarpour, and S. Member, "Artificial proprioceptive feedback for myoelectric control," *IEEE Trans. Neural Syst. Rehabil. Eng.*, vol. 23, no. 3, pp. 498–507, May 2015.
- [39] C. L. Taylor and R. J. Schwarz, "The anatomy and mechanics of the human hand," *Artif. Limbs*, vol. 2, no. 2, pp. 22–35, 1955.
- [40] M. Wedyan, A. Al-Jumaily, F. Alnajjar, P. M. Muhammed, and S. Shimoda, "A wearable robotics assistive device: Design, technical solutions, and implementation," in *Proc. Int. Conf. Electr. Comput. Technol. Appl.*, Jan. 2017, pp. 1–5.
- [41] J. Iqbal and K. Baizid, "Stroke rehabilitation using exoskeleton-based robotic exercisers: Mini review," *Biomed. Res.*, vol. 26, no. 1, pp. 197–201, 2015.
- [42] V. Patel, J. Craig, M. Schumacher, M. K. Burns, I. Florescu, and R. Vinjamuri, "Synergy repetition training versus task repetition training in acquiring new skill," *Frontiers Bioeng. Biotechnol.*, vol. 5, pp. 1–13, Feb. 2017.
- [43] E. Todorov and Z. Ghahramani, "Analysis of the synergies underlying complex hand manipulation," in *Proc. 26th Annu. Int. Conf. IEEE Eng. Med. Biol. Soc.*, 2005, vol. 2, pp. 4637–4640.
- [44] F. Ficuciello, D. Zaccara, and B. Siciliano, "Synergy-based policy improvement with path integrals for anthropomorphic hands," in *Proc. IEEE Int. Conf. Intell. Robots Syst.*, Nov. 2016, pp. 1940–1945.
- [45] A. Provenzale, F. Cordella, L. Zollo, A. Davalli, R. Sacchetti, and E. Guglielmelli, "A grasp synthesis algorithm based on postural synergies for an anthropomorphic arm-hand robotic system," in *Proc. 5th IEEE RAS & EMBS Int. Conf. Biomed. Robot. Biomechatronics*, 2014, pp. 958–963.
- [46] N. Garcia, R. Suarez, and J. Rosell, "Planning hand-arm grasping motions with human-like appearance," in *Proc. IEEE/RSJ Int. Conf. Intell. Robots Syst.*, 2018, pp. 3517–3522.
- [47] F. Ficuciello, G. Palli, C. Melchiorri, and B. Siciliano, "Experimental evaluation of postural synergies during reach to grasp with the UB hand IV," in *Proc. IEEE Int. Conf. Intell. Robots Syst.*, 2011, pp. 1775–1780.
- [48] A. Ajoudani, S. B. Godfrey, M. Catalano, G. Grioli, N. G. Tsagarakis, and A. Bicchi, "Teleimpedance control of a synergy-driven anthropomorphic hand," in *Proc. IEEE Int. Conf. Intell. Robots Syst.*, 2013, pp. 1985–1991.

- [49] T. Wimböck, B. Jahn, and G. Hirzinger, "Synergy level impedance control for multifingered hands," in *Proc. IEEE Int. Conf. Intell. Robot. Syst.*, 2011, pp. 973–979.
- [50] R. Meattini, S. Benatti, U. Scaria, D. De Gregorio, L. Benini, and C. Melchiorri, "An sEMG-based human–robot interface for robotic hands using machine learning and synergies," *IEEE Trans. Compon. Packag. Manuf. Technol.*, vol. 8, no. 7, pp. 1149–1158, Jul. 2018.
- [51] P. K. Artemiadis and K. K. Kyriakopoulos, "EMG-based control of a robot arm using low-dimensional embeddings," *IEEE Trans. Robot.*, vol. 26, no. 2, pp. 393–398, Apr. 2010.
- [52] V. Patel, M. Burns, Z. H. Mao, N. E. Crone, and R. Vinjamuri, "Linear and nonlinear kinematic synergies in the grasping hand," *Bioeng. Biomed. Sci.*, vol. 5, no. 2, pp. 1–8, 2015.
- [53] D. Pei, V. Patel, M. Burns, R. Chandramouli, and R. Vinjamuri, "Neural decoding of synergy-based hand movements using electroencephalography," *IEEE Access*, vol. 7, pp. 18155–18163, Jan. 2019.
- [54] M. Borghetti, E. Sardini, and M. Serpelloni, "Sensorized glove for measuring hand finger flexion for rehabilitation purposes," *IEEE Trans. Instrum. Meas.*, vol. 62, no. 12, pp. 3308–3314, Dec. 2013.
- [55] C. Preetham, G. Ramakrishnan, S. Kumar, A. Tamse, and N. Krishnapura, "Hand talk-implementation of a gesture recognizing glove," in *Proc. Texas Instrum. India Educ. Conf.*, 2013, pp. 328–331.
- [56] A. Syed, Z. T. H. Agasbal, T. Melligeri, and B. Gudur, "Flex sensor based robotic arm controller using micro controller," *J. Softw. Eng. Appl.*, vol. 5, no. 5, pp. 364–366, 2012.



Martin K. Burns (S'19) received the B.S. degree in biomedical engineering and the M.E. degree in engineering management in 2015 from the Stevens Institute of Technology, Hoboken, NJ, USA, where he is currently working toward the Ph.D. degree with the Biomedical Engineering Department. From 2011 to 2012, he worked with the Merck & Co., prototyping high-throughput laboratory robotics, and in 2013, worked for Stryker, designing implants in Advanced Concept Development. He is currently a Research Assistant with the Stevens Institute of Technology. His research interests include robotics and control systems for assistive and rehabilitative robotics and brain–machine interfaces. His work is supported by the New Jersey Health Foundation, the National Science Foundation, the Innovation and Entrepreneurship Doctoral Fellowship, and the Stevens Excellence Doctoral Fellowship.



Dingyi Pei (S'18) received the B.S. degree in biomedical engineering from the Tianjin University, China, in 2016, and the M.E. degree in biomedical engineering from the Stevens Institute of Technology, Hoboken, NJ, USA, in 2018, where he is currently working toward the Ph.D. degree in biomedical engineering. Her undergraduate and graduate research projects consisted of prosthetic control methods, brain–computer interfaces, biosignal detection circuit designs, biosignal, and medical image processing.

Pei received Steven's Provost Doctoral Fellowship for her current research. She also received the third prize in International Contest of Applications in Nano-Micro Technologies in 2014.



Ramana Vinjamuri (M'08–SM'11) received the B.S. degree in electrical engineering from the Kakatiya University, India, in 2002, the M.S. degree in electrical engineering from the Villanova University, Villanova, PA, USA, in 2004, and the Ph.D. degree in electrical engineering from the University of Pittsburgh, Pittsburgh, PA, USA, in 2008.

He was a Research Associate with the Department of Physical Medicine and Rehabilitation, University of Pittsburgh, PA, USA, from 2008 to 2012. He then was a Research Assistant and Professor with the Department of Biomedical Engineering, Johns Hopkins University, Baltimore, MD, USA, from 2012 to 2013. He then joined the Department of Biomedical Engineering, Stevens Institute of Technology, Hoboken, NJ, USA, as an Assistant Professor in 2013. He is currently a Harvey N Davis Distinguished Assistant Professor with the Department of Biomedical Engineering, Stevens Institute of Technology.

Dr. Vinjamuri received the NSF CAREER Award in 2019.